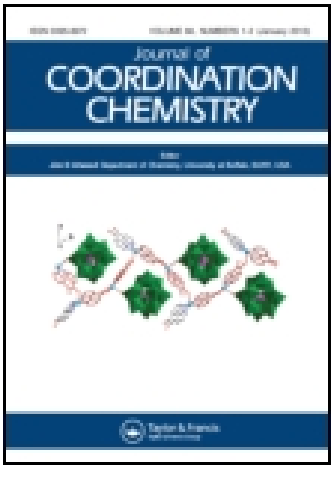

Journal of Coordination Chemistry
Publication details, including instructions for authors and subscription information:
http://www.tandfonline.com/loi/gcoo20

Synthesis, spectroscopic, and biological studies on copper(II) complexes containing equatorial-apical chloride bridges: crystal structure of $[Cu_2(\mu\text{-}Cl)_2(O\text{-}2\text{-butoxyethylpyridine-2-carboximidate})_2Cl_2]$

R.K. Bindiya Devi[a], S. Pramodini Devi[a], R.K. Bhubon Singh[a], R.K. Hemakumar Singh[a], Toka Swu[b], W. Radhapiyari Devi[c] & CH. Brajakishore Singh[c]

[a] Department of Chemistry, Manipur University Canchipur, Imphal, India

[b] Department of Chemistry, Pondicherry University, Puducherry, India

[c] Department of Biotechnology, Institute of Bioresources and Sustainable Development, Imphal, India

Accepted author version posted online: 10 Mar 2014.Published online: 07 Apr 2014.

To cite this article: R.K. Bindiya Devi, S. Pramodini Devi, R.K. Bhubon Singh, R.K. Hemakumar Singh, Toka Swu, W. Radhapiyari Devi & CH. Brajakishore Singh (2014) Synthesis, spectroscopic, and biological studies on copper(II) complexes containing equatorial-apical chloride bridges: crystal structure of $[Cu_2(\mu\text{-}Cl)_2(O\text{-}2\text{-butoxyethylpyridine-2-carboximidate})_2Cl_2]$, Journal of Coordination Chemistry, 67:5, 891-909, DOI: 10.1080/00958972.2014.902449

To link to this article: http://dx.doi.org/10.1080/00958972.2014.902449

Journal of Coordination Chemistry, 2014
Vol. 67, No. 5, 891–909, http://dx.doi.org/10.1080/00958972.2014.902449

Synthesis, spectroscopic, and biological studies on copper(II) complexes containing equatorial–apical chloride bridges: crystal structure of $[Cu_2(\mu\text{-}Cl)_2(O\text{-}2\text{-}butoxyethylpyridine\text{-}2\text{-}carboximidate)_2Cl_2]$

R.K. BINDIYA DEVI†, S. PRAMODINI DEVI†, R.K. BHUBON SINGH†, R.K. HEMAKUMAR SINGH*†, TOKA SWU‡, W. RADHAPIYARI DEVI§ and CH. BRAJAKISHORE SINGH§

†Department of Chemistry, Manipur University Canchipur, Imphal, India
‡Department of Chemistry, Pondicherry University, Puducherry, India
§Department of Biotechnology, Institute of Bioresources and Sustainable Development, Imphal, India

(*Received 11 September 2013; accepted 9 January 2014*)

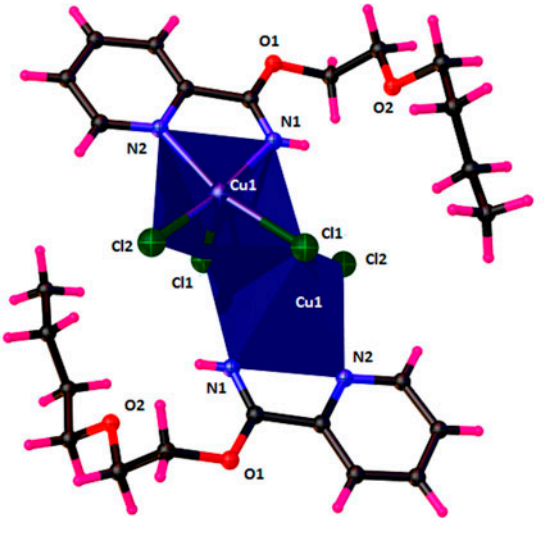

Three new $[Cu_2(\mu\text{-}Cl)_2(O\text{-}2\text{-}alkoxyethylpyridine\text{-}2\text{-}carboximidate)_2Cl_2]$ complexes, where alkoxy = methoxy, ethoxy, and butoxy, were synthesized and characterized by elemental analyses, FTIR spectra, electronic spectra, EPR, conductance, magnetic moment, powdered X-ray powder diffraction, and X-ray single-crystal diffraction. The three complexes contain chloride as a bridging ligand and in each complex the planar bidentate ligand binds the metal ion via the pyridine-N and the NH of

*Corresponding author. Email: rkhemakumar@rediffmail.com

the imino ether group. The X-ray crystal structure of $[Cu_2(\mu\text{-}Cl)_2(O\text{-}2\text{-}butoxyethylpyridine\text{-}2\text{-}carboximidate)_2Cl_2]$ shows that it crystallizes as a centrosymmetric dinuclear species in which each copper (II) is in a distorted square pyramid. Magnetic field-induced partial molecular alignment has been observed in polycrystalline samples of **2** and **3** when cooled in a magnetic field of 1 T at 77 K. The interaction of these complexes with Calf thymus DNA has been explored and the values of binding constant, K_b for **1**, **2**, and **3** are 1.524×10^3, 5.587×10^3, and 6.362×10^3 $(ML^{-1})^{-1}$, respectively. Complexes were screened for antimicrobial activities by the agar well diffusion technique.

Keywords: 2-Cyanopyridine; Bridging ligand; EPR; Triclinic; Field-induced

1. Introduction

Studies on the molecular structure of metal complexes and their biological activities have received much attention from inorganic chemists. DNA binding studies are also very important for the development of new therapeutic and DNA probes [1]. For understanding the functions of nucleic acids in biological systems and the action mechanism of the DNA-targeted drugs, it is very important to understand the interactions between cationic metal complexes containing multidentate aromatic ligands with DNA [2, 3]. These metal complexes can bind to DNA according to three possible patterns: (1) electrostatic interaction, in which the metal complexes are electrostatically adsorbed on the phosphates of DNA, (2) intercalative binding, in which the metal complexes intercalate into the base pairs of the double-stranded DNA, and (3) groove binding, in which the metal complexes interact with the grooves of DNA [3–5]. The discovery of cisplatin offers a good result in the treatment of cancer patients; however, side effects such as nephrotoxicity, neurotoxicity, nausea, and vomiting were found [6]. As a result, there is a continuous search for metal-based drugs which are less toxic. Copper, being a natural constituent of the cell nuclei, should be much less toxic than non-endogenous metals; therefore the search for the new drugs based on copper, which has been suggested to play a key role in structural organization [7] and function [8] of chromosomes, is reasonable. A large number of studies have focused on the biological role of copper(II) and its synergetic activity with drugs [9]. Indeed, copper(II) chelates interact with biological systems to reveal antineoplastic activity [10–12], and the effectiveness of many anticancer agents depends on the mode and affinity of their binding with DNA [13]. Antifungal and antibacterial properties of a range of copper(II) complexes have been evaluated against several pathogenic fungi and bacteria [14, 15]. Coordination compounds of both oxidation states (+1,+2) have been extensively used in metal-mediated DNA cleavage through the generation of hydrogen abstracting activated oxygen species [16, 17]. Copper(II) complexes have also been shown to bring about photocleavage of DNA as well as RNA, and DNA scission via phosphodiester transesterification [18, 19]. There are also reports of copper complexes cleaving DNA hydrolytically and several other copper-based synthetic nucleases [20, 21]. Recently, Chetana *et al*. have reported oxidative DNA cleavage, cytotoxicity, and antimicrobial studies of L-ornithine copper(II) complexes [22].

Pyridine derivatives play a significant role in the biological materials, e.g. in the coenzyme of NAD, NADP, and pyridoxal phosphate. Another pyridine derivative is the tryptophan metabolite of picolinic acid which has a role in the absorption of zinc [23]. We have been studying coordination compounds of 2-cyanopyridine, as this potentially bidentate ligand is primarily a pyridine ligand retaining hydrogen bonding facilities after coordinating

through pyridyl-N. Reactions of alcohols and water with pyridine-2-carbonitrile in the presence of metal(II) salts results in the formation of complexes of pyridine-2-carboxamide or O-alkylpyridine-2-carboximidate [24–26]. Jamnicky *et al*. [27] reported the methanolysis of pyridine-2-carbonitrile in the coordination sphere of copper, cobalt, and nickel complexes, and determined the X-ray single-crystal structure of [Ni(O-methylpyridine-2-carboximidate)$_3$Br$_2$·4H$_2$O. There were no chloride bridges in the structure of the complexes, but in our synthesized complexes there are two chlorides which bridge both coppers. They did not investigate biological properties of the complexes. Thus, bearing in mind the importance of copper complexes and pyridine, in the present investigation, we have chosen to synthesize copper(II) complexes of 2-cyanopyridine and to quantify the binding abilities of these complexes with DNA in aqueous solution. The major advantage of these complexes is their solubility in water since there has been a growing concern in the study of water-soluble transition metal complexes as such complexes are rare and could enhance biological compatibility *in vivo*.

2. Experimental

2.1. *Materials and physical measurements*

Copper(II) chloride dihydrate crystal pure (Merck, India), highly pure 2-pyridinecarbonitrile (Sigma Aldrich), and the solvents used in this work were of analytical grade and used without purification. CT-DNA and Tris–HCl molecular biological grade were obtained from Merck (India). Ethidium bromide (EB) was obtained from Sigma. Deionized, sonicated triple-distilled H$_2$O was used throughout the experiment. Nutrient agar (NA) was obtained from Hi-Media. IR spectra were recorded using a Shimadzu FTIR-8400S. Electronic spectra were recorded on a Perkin Elmer UV–vis Lamda 35 spectrophotometer. Microanalyses (C, H, and N) were carried out using a Perkin Elmer 2400 model elemental analyzer. EPR spectra of the complex were recorded on a JEOL, JES-FA 200 EPR spectrometer, X-band microwave unit. TEMPOL was used as the field marker. The room temperature (RT) magnetic moment (μ_{eff}) was measured using a Sherwood Scientific susceptibility balance. Molar conductance in DMSO was measured at RT on a Eutech instrument Con 510 conductivity meter. The thermogram was recorded on a Perkin Elmer STA 6000 machine. Luminescent properties were investigated with a Perkin Elmer LS55 fluorescence spectrophotometer. Cyclic voltammetry (CV) was performed on a CH602C electrochemical analyzer. X-ray powder diffraction (XRD) measurements were carried out in a PANalytical powder diffractometer (X' Pert PRO) using CuK$_\alpha$ (1.540 Å) radiation fitted with a Ni filter.

2.2. *Synthesis of complexes*

2.2.1. Synthesis of [Cu$_2$(μ-Cl)$_2$(O-2-methoxyethylpyridine-2-carboximidate)$_2$Cl$_2$] (1).

[Cu$_2$(μ-Cl)$_2$(O-2-methoxyethylpyridine-2-carboximidate)$_2$Cl$_2$] was prepared by refluxing a mixture of CuCl$_2$·2H$_2$O (0.173 g, 1 mM) and 2-cyanopyridine (0.104 g, 1 mM) on a water bath for 8 h in 2-methoxyethanol and evaporating the solution to a minimum volume. Block blue crystalline complex was obtained after keeping the resulting solution at RT for 10–15 days. The complex so obtained was washed with mother solvent and dried in air. Color –

blue, Yield 75%, m.p. 194 °C, magnetic moment, μ_{eff} (1.89 BM), elemental analysis for $C_{18}H_{24}Cl_4Cu_2N_4O_4$ (molar mass: 629.45 gM^{-1}), Calcd (%): C, 34.31; H, 3.81; N, 8.89; Cu, 20.18. Found (%): C, 34.28; H, 3.79; N, 8.78; Cu, 20.07. IR (KBr, cm^{-1}) υ: 3308, 3178, 2982, 1649, 1599, 1421, 1359, 1230, 1197, 1174, 1016, 987, 324, 289, 241, 210.

2.2.2. Synthesis of $[Cu_2(\mu\text{-}Cl)_2(O\text{-}2\text{-}ethoxyethylpyridine\text{-}2\text{-}carboximidate)_2Cl_2]$ (2). This complex was synthesized by the same procedure as described above for **1** from $CuCl_2{\cdot}2H_2O$ (0.173 g, 1 mM) and 2-cyanopyridine (0.104 g, 1 mM) in 2-ethoxyethanol solvent. Color – blue, Yield 70%, m.p. 230 °C, magnetic moment, μ_{eff} (1.90 BM), elemental analysis for $C_{20}H_{28}Cl_4Cu_2N_4O_4$ (molar mass: 657.45 gM^{-1}), Calcd (%): C, 36.50; H, 4.26; N, 8.52; Cu, 19.33. Found (%): C, 36.43; H, 4.22; N, 8.46; Cu, 19.30. IR (KBr, cm^{-1}) υ: 3360, 3086, 2974, 2889, 1653, 1597, 1462, 1402, 1359, 1267, 1178, 1147, 1049, 1018, 941, 866, 451, 314, 285, 264, 241, 210.

2.2.3. Synthesis of $[Cu_2(\mu\text{-}Cl)_2(O\text{-}2\text{-}butoxyethylpyridine\text{-}2\text{-}carboximidate)_2Cl_2]$ (3). The complex was also synthesized by the same procedure as described above from $CuCl_2{\cdot}2H_2O$ (0.173 g, 1 mM) and 2-cyanopyridine (0.104 g, 1 mM) in 2-butoxyethanol. For this complex, bluish-green single crystals suitable for X-ray diffraction were obtained by slow evaporation of the solution. Yield 73%, m.p. 180 °C, magnetic moment, μ_{eff} (1.95 BM), elemental analysis for $C_{24}H_{36}Cl_4Cu_2N_4O_4$ (molar mass: 713.45 gM^{-1}), Calcd (%): C, 40.36; H, 5.04; N, 7.84; Cu, 17.81%. Found (%): C, 40.29; H, 5.01; N, 7.79; Cu, 17.75. FTIR (KBr, cm^{-1}) υ: 3311, 3097, 2953, 2862, 1662, 1597, 1410, 1373, 1195, 1161, 1124, 979, 914, 810, 761, 557, 339, 322, 270, 243, 216. A representative reaction scheme for the synthesis of the complexes is shown in scheme 1.

2.3. *Crystallographic data collection and refinement*

The crystal structure of **3** was collected on an Oxford Diffractometer (Xcalibur, Eos diffractometer) Gemini-E CCD system with graphite-monochromated MoKα ($\lambda = 0.71073$) radiation at 296(2) K. Data reduction and absorption correction were performed with the CrysAlis program Version 1.171.34.44 [28]. The structure of the complex was solved by direct methods using the SHELX-97 software [29]. Empirical absorption correction using spherical harmonics was implemented in SCALE3 ABSPACK scaling algorithm. The

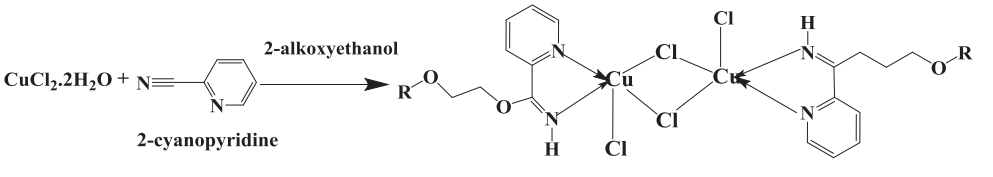

where R = CH_3, CH_2CH_3 and $CH_2CH_2CH_2CH_3$

Scheme 1. Reaction.

non-H atoms were anisotropically refined using the full-matrix least square on F^2. All hydrogens were placed at calculated positions and refined riding on the parent with atom–hydrogen lengths and isotropic displacement parameters. Molecular graphics were made by using OLEX-2 [30]. Crystallographic details of the data collection and structure refinement are summarized in table 1. Selected bond lengths (Å) and angles (°) are given in table 2.

2.4. *DNA-binding studies*

DNA-binding experiments were carried out in tris buffer containing 5 mM (Tris–HCl) and 50 mM NaCl (pH 7.4) using a solution of calf thymus CT-DNA which gave a ratio of UV–vis absorbance at (A_{260}/A_{280}) of ca. 1.8, indicating the DNA was sufficiently protein-free [31]. The concentration of DNA was determined at 260 nm and the value of molar absorptivity coefficient was taken to be 6600 M^{-1} cm^{-1} [32]. The intrinsic binding constant, K_b, was determined by the following equation:

$$[\mathrm{DNA}]/(\varepsilon_a - \varepsilon_f) = [\mathrm{DNA}]/(\varepsilon_b - \varepsilon_f) + [K_b(\varepsilon_b - \varepsilon_f)]^{-1} \quad (1)$$

where ε_a, ε_f, and ε_b correspond to apparent, free, and bound metal complexes extinction coefficients, respectively. In the plot [DNA]/($\varepsilon_a - \varepsilon_f$) *versus* [DNA], K_b is the ratio of the slope to the intercept.

Thermal denaturation studies were carried out by monitoring the absorption intensity of CT-DNA (200 μM) at 260 nm from 25 to 98 °C using a Perkin-Elmer UV–vis Lamda 35 spectrophotometer equipped with a Peltier temperature-controlling programmer (PTP6), both in the absence and presence of varying concentrations of the complexes.

Competitive binding studies of the complexes with EB to DNA were investigated by fluorescence spectroscopy. The fluorescence spectra were recorded at RT with an excitation at 274 nm and the emission between 500 and 700 nm. The DNA–EB complex was prepared by adding 1.3 μM EB and 2.5 μM DNA in tris buffer. The effect of complexes on the fluorescence of

Table 1. Crystal data and structure refinement for **3**.

CCDC	928659
Empirical formula	$C_{24}H_{36}Cl_4Cu_2N_4O_4$
Formula mass	713.45
Crystal system	Triclinic
Space group	*P*
a/Å	9.4169(5)
b/Å	9.4996(6)
c/Å	9.9383(4)
α/°	115.384(5)
β/°	98.312(4)
γ/°	91.459(5)
V/Å^3	790.97(7)
Z	1
D_x/Mg m^{-3}	1.498
μ/mm^{-1}	1.72
F (0 0 0)	366
R_{int}	0.020
$I > 2\sigma(I)$	2459
*R*1, *wR*2	0.027, 0.078
Temp/K	298

Table 2. Bond distances (Å) and angles (°) in the metal coordination spheres for **3**.

Cu1–N1	1.972(2)
Cu1–N2	2.0642(18)
Cu1–Cl1i	2.7027(7)
Cl1–Cu1i	2.7027(7)
Cu1–Cl1	2.2748(6)
Cu1–Cl2	2.2375(6)
Cl1–Cu1–Cl1i	96.89(2)
Cl2–Cu1–Cl1	94.98(3)
Cl2–Cu1–Cl1i	100.57(3)
N1–Cu1–Cl1i	88.21(7)
N1–Cu1–Cl1	88.71(7)
N1–Cu1–Cl2	169.97(7)
N1–Cu1–N2	79.43(8)
N2—Cu1–Cl1	165.51(6)
N2–Cu1–Cl1i	91.08(5)
N2–Cu1–Cl2	95.43(5)
Cu1–Cl1–Cu1i	83.11(2)

Note: Symmetry code: (i) $-x+1, -y, -z+1$.

DNA–EB complex was studied by varying the concentration of the complexes. The apparent binding constant (K_{app}) was calculated using the following equation [33]:

$$K_{EB}[EB] = K_{app}[Complex]$$

where the complex concentration was the value at a 50% reduction of the fluorescence intensity of EB and $K_{EB} = 1.0 \times 10^7$ $(ML^{-1})^{-1}$, [EB] = 1.3 μM L^{-1}.

The electrochemical studies were performed by CV in the potential range from 0.6 to −0.8 V in tris buffer (pH 7.4) (using a glassy carbon working electrode), Pt wire as counter electrode, and Ag/AgCl as reference electrode. The experiments were carried out in 0.001 M complex solution in the absence and presence of CT-DNA.

2.5. *Antimicrobial activity*

In vitro antibacterial activity was assessed by agar well diffusion using 20 mL of sterile NA against *Proteus mirabilis*, *Klebsiella pneumoniae*, *Escherichia coli*, *Salmonella paratyphi*, and *Pseudomonas aeruginosa* [34]. The dilution plate method was used to enumerate micro-organisms (10^5 Cells mL^{-1}) for 24 h [35, 36]. The samples were diluted 5 mg mL^{-1} in DMSO. The dilutions of the sample concentration were deposited 20 μL on the inoculated well and left for 10 min at RT for the extract diffusion. Negative control was prepared using DMSO. Ciprofloxacin (Hi-Media) for bacteria served as positive control. The plates were inoculated with bacteria and incubated at 37 °C for 24 h. The experiment was repeated four times and the average results were recorded. The antimicrobial activity was determined by measuring the diameter of the inhibition zone (mm) around the well. The susceptibility of microbes was determined by minimum inhibitory concentration (MIC) determination [37]. The MICs of the samples were determined by serial dilution against the micro-organisms. The minimum concentrations at which no visible growth was observed were defined as the MICs, expressed in mg mL^{-1}.

3. Results and discussion

The synthesized complexes are characterized by analytical and spectral techniques. These complexes are highly stable, non-hygroscopic, and soluble in solvents like water, methanol, ethanol, DMF, DMSO, etc. Elemental analysis data are in agreement with the presented formula. Conductivity measurements of these complexes in DMSO (0.001 M) indicate that the complexes are 1 : 1 electrolytes ($\Lambda_M = 50–60\ \Omega^{-1}cm^2\ M^{-1}$). All the complexes are paramagnetic at RT. The magnetic moment values are 1.89–1.95 BM at RT, typical of magnetically dilute copper(II) complexes where the individual copper(II) ions are separated from each other (no intermolecular magnetic interaction). The magnetic moment values higher than spin-only values (1.73 BM) of Cu^{2+} might be due to orbital contributions [38–41].

3.1. *IR spectra*

IR spectra of **1**–**3** are illustrated in Supplementary material, see online supplemental material at http://dx.doi.org/10.1080/00958972.2014.902449. The IR spectrum of the pyridine-2-carbonitrile exhibits ν(C≡N) at 2237 cm^{-1} but after complex formation there is no band at 2237 cm^{-1}, suggesting the absence of nitrile bands in these complexes and conversion of nitrile to imino ether [27]. The bands belonging to ν(C=N) have a small shift to 1662–1649 cm^{-1} for the complexes compared to ligand at 1650 cm^{-1}, presumably due to a change in C=N bond order, on coordination through nitrogen, facilitated by transfer of electron density from the C–O–C moiety. The electron density on the N=C–O–C fragment of the imino ether group is more delocalized in the complexes and =C–O bond order is raised [24, 27, 42]. Bands at 1373–1359 cm^{-1} can be assigned to ν(=C–O–) stretching mixed with δ (NH) of the imino ether group. Strong and broad ν(NH) are observed at 3308 for **1**, 3360 cm^{-1} for **2**, and 3311 cm^{-1} for **3**. The presence of a strong band at ~1195–1197 cm^{-1} can be attributed to wagging of (O–CH_3). The complexes exhibit a ν_a(COC) stretch at ca. 1161–1147 cm^{-1} and ν_s(COC) at ca. 987–979 cm^{-1}. The N→Cu bonding was supported by ν(Cu–N) bands at ~314–324 cm^{-1} for complexes [27].

3.2. *Electronic spectra*

The electronic spectra of **1–3** recorded in solid state and DMF solution of all the three complexes have similar absorption patterns, displaying two bands at 200–900 nm. The sharp and strong high-energy band at 378 nm for **1**, 379 nm for **2**, and 376 nm for **3** are assigned to charge transfer from pyridine to copper (LMCT). A broad band in the visible region 762 nm for **1**, 766 nm for **2**, and 766 nm for **3** correspond to d–d transitions, revealing the presence of distorted square-pyramidal copper [43]; representative spectra of the complexes are shown in Supplementary material.

3.3. *EPR studies*

The EPR spectra of **1–3** were recorded both in the solid and DMF solution at RT and liquid nitrogen temperatures (LNT), as shown in figure 1 for **2**. The EPR spectra of the complexes in DMF at LNT indicate a well-defined hyperfine structure of four lines due to coupling of the electron with the nuclear spin $I = 3/2$ of copper. The $g_{\|}$ and $g_{\perp}$ (tables 3 and 4) values are computed from the spectra using TEMPOL as field marker. Kivelson and Neiman [44] reported that $g_{\|}$ less than 2.3 indicates significant covalent character and greater than 2.3

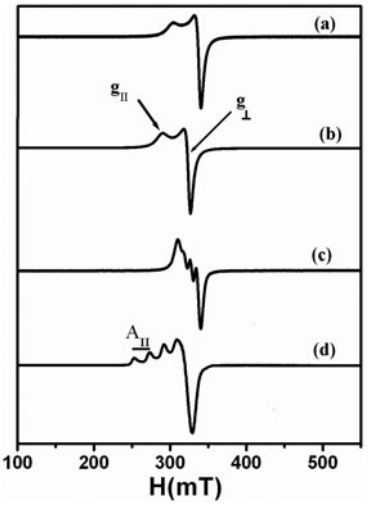

Figure 1. EPR spectra of **2**; (a) solid LNT, (b) solid RT, (c) liquid LNT, and (d) liquid RT.

ionic character for metal ligand bonds. Since the g values are less than 2.3, this shows significant covalent character in the metal–ligand bonding. Moreover the trend $g_{\parallel} > g_{\perp} > 2.0023$ shows that the unpaired electrons lie predominantly in the d_{x2-y2} orbital of Cu(II) and spectral features are characteristic of axial symmetry [45]. The EPR parameters and d–d transition energies are used to evaluate the bonding parameters α^2, β^2, and γ^2, which may be regarded as measures of covalence of the in-plane σ-bonding, the in-plane π-bonding, and out-of-plane π-bonding, respectively. The in-plane σ-bonding parameters α^2 is calculated using the expression [44, 46],

$$\alpha^2 = -(A_{\parallel}/0.036) + (g_{\parallel} - 2.0023) + 3/7\,(g_{\perp} - 2.0023) + 0.04$$

The orbital reduction factors $K_{\parallel}$ and $K_{\perp}$ are estimated from the simplified expression [47],

$$K_{\parallel}{}^2 = (g_{\parallel} - 2.0023)E_{\mathrm{d-d}}/8\lambda_0$$

$$K_{\perp}{}^2 = (g_{\perp} - 2.0023)E_{\mathrm{d-d}}/2\lambda_0$$

Table 3. EPR parameter for the copper(II) complexes in the solid state at 300 K.

Compound	$g\parallel$	$g_{\perp}$	g_{av}	G
CuL1	2.2293	2.0686	2.1222	3.3425
CuL2	2.2360	2.0694	2.1249	3.4005
CuL3	2.2505	2.0644	2.1264	3.8843

[L1](O-2-methoxyethylpyridine-2-carboximidate), [L2](O-2-ethoxyethylpyridine-2-carboximidate), [L3] (O-2-butoxyethylpyridine-2-carboximidate).

Table 4. EPR and bonding parameters for copper(II) complexes in DMF solution.

Compound	Solution	Temp (K)	$A_{\parallel}$ (G)	$A_{\perp}$ (G)	A_{av} (G)	$g_{\parallel}$ (G)	$g_{\perp}$ (G)	g_{av} (G)	α^2	β^2	γ^2	K	$K_{\parallel}$	$K_{\perp}$	G
CuL1	DMF	300				2.2493	2.0653	2.1266							
		77	148	32	71	2.2208	2.0688	2.1194	0.7011	0.9385	1.0355	0.3349	0.6579	0.7259	3.209
CuL2	DMF	300				2.2533	2.0597	2.1242							
		77	149	35	73	2.2201	2.0732	2.1232	0.7025	0.9351	1.0698	0.3440	0.6569	0.7516	3.043
CuL3	DMF	300				2.2464	2.0602	2.1223							
		77	148	35	72	2.2202	2.0707	2.1143	0.6987	0.9402	1.0541	0.3318	0.6569	0.7364	3.111

[L1] (O-2-methoxyethylpyridine-2-carboximidate), [L2] (O-2-ethoxyethylpyridine-2-carboximidate), [L3] (O-2-butoxyethylpyridine-2-carboximidate).

where $K_{\parallel} = \alpha^2\beta^2$, $K_{\perp} = \alpha^2\gamma^2$, and λ_0 represents the one electron spin–orbital coupling constant for the free ion (828 cm^{-1}). Significant information about the nature of bonding in the copper(II) complexes can be derived from the relative magnitudes of $K_{\parallel}$ and $K_{\perp}$. In case of pure in-plane σ-bonding, $K_{\parallel} = K_{\perp} = 0.77$ and for in-plane π-bonding, $K_{\parallel} < K_{\perp}$ while for out-of-plane π-bonding, $K_{\parallel} > K_{\perp}$ [48]. Furthermore, α^2, β^2, and γ^2 have values much less than 1 (the value expected for 100% ionic character of the bonds, this value decreases with increasing covalent bonding). The complexes show $K_{\parallel} > K_{\perp}$ (table 5) in DMF solvent, which indicates the presence of more out-of-plane π-bonding than the in-plane π-bonding.

The EPR parameters (g-values) are close to those reported for four-coordinate planar complexes at 300 K, suggesting that these complexes possess near square-planar geometry [46, 49]. The EPR spectra of solid complexes consist of $g_{\parallel} = 2.2505$ with a typical bell-like line shape and an intense line corresponding to $g_{\perp} = 2.0644$, having a typical derivative line shape. A typical RT spectrum of **2** and **3** are shown in Supplementary material. When the sample was cooled to 77 K, with the sample-loaded cavity in a magnetic field of 0.3 T, the relatively weak line grew considerably in intensity, and also its line shape changed from "absorption like" to "dispersion like." Furthermore, the intensity of the perpendicular component had been correspondingly reduced. To determine whether these features are due to field-induced alignment, the spectra are recorded at 77 K under the following conditions.

(1) Samples were cooled at zero magnetic field (zero field cooling, ZFC).
(2) Samples were cooled at 77 K at 1 T magnetic field, and subsequently scanned in the relevant range (field cooled, FC).

EPR spectra, recorded under ZFC, are identical to that recorded at RT (except for an overall increase in intensity due to the 1/T behavior). An important observation is the change in the shape of the parallel component only in FC samples. The new features leveled off with FC at 1 T. These field-induced alignments are most prominent in **2** and **3**, but less prominent in **1**. The degree of alignment under the conditions ($H = 0.4$ T) was roughly estimated from the asymmetry of the parallel component, i.e. the amplitude ratio of the derivative line with the lower value being in the numerator. This was found to be ca. 20%. The simulated spectrum with 20% ordering agreed well with the experimental spectrum. It is relevant to mention here that in C_7Cu metallo mesogens, nearly 100% alignment was observed and the quartet hyperfine structure was well resolved despite the higher copper concentration (undiluted), in contrast to the present study where the hyperfine structure disappeared due to the large spin–spin interaction [50, 51]. We believe that this intrinsic difference in the metal–metal interaction is responsible for not allowing a higher degree of field induced ordering in the present case.

3.4. *Crystal structure description of 3*

Bluish green crystals were obtained from 2-butoxyethanol. An ORTEP view of the neutral complex along with the atomic numbering scheme is shown in figure 2 and selected bond lengths and angles are given in tables 1 and 2, respectively. The complex crystallizes as a centrosymmetric dinuclear species in which each copper(II) is in a distorted square-pyramidal structure having the formula [Cu(μ-Cl)(O-2-butoxyethylpyridine-2-carboximidate)Cl]. In

Table 5. Cyclic voltammetric behavior of **1–3** in 5 mM Tris HCl/50 mM NaCl in the absence and presence of CT-DNA.

		Cu(II)/Cu(I) Peaks (I)							Cu(I)/Cu(0) Peaks (II)						
Complex	[DNA] (μM)	E_{pc} (V)	E_{pa} (V)	I_{pc} (μA)	I_{pa} (μA)	ΔE_p (V)	$E_{1/2}$ (V)	I_{pa}/I_{pc}	E_{pc} (V)	E_{pa} (V)	I_{pc} (μA)	I_{pa} (μA)	ΔE_p (V)	$E_{1/2}$ (V)	I_{pa}/I_{pc}
1	0	−0.263	0.185	13.11	10.82	0.448	−0.039	0.825	−0.372	−0.005	16.93	37.76	0.367	−0.188	2.230
	100	−0.265	0.130	14.09	12.86	0.395	−0.067	0.928	−0.388	−0.010	15.63	39.23	0.378	−0.199	2.509
2	0	−0.276	0.250	10.79	7.49	0.536	−0.018	0.681	−0.417	−0.001	14.20	15.89	0.415	−0.209	1.823
	100	−0.288	0.213	11.38	8.01	0.482	−0.028	0.724	−0.440	−0.010	13.74	31.74	0.430	−0.225	2.310
3	0	−0.320	0.228	7.86	4.29	0.548	−0.046	0.545	−0.485	−0.014	9.76	8.59	0.471	−0.249	0.880
	100	−0.321	0.216	6.98	4.51	0.521	−0.060	0.646	−0.513	−0.025	8.63	9.14	0.488	−0.269	1.059

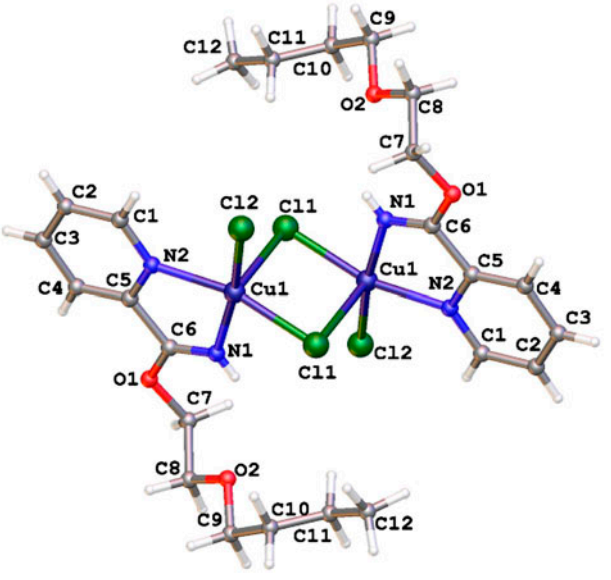

Figure 2. The coordination environment of copper in the structure of **3** with ellipsoids at 50% probability.

the complex, the ligand is a bidentate chelate bonded through N (pyridine) and N (imino ether group) having a five member chelate ring. The four chlorides Cl1, $Cl1^{i}$, Cl2, and $Cl2^{i}$ contribute four negative charges which neutralize the +4 charges of the two coppers. One chloride in each asymmetric unit bridges two coppers, whereas the other chloride is terminal as shown in figure 2. In the structure, the square plane of the metal is occupied by N (pyridine), N (imino ether group), bridging Cl(1), and terminal Cl(2); each bridging Cl^{-} occupies equatorial–apical bridges by edge sharing for each asymmetric unit. The copper is displaced from the mean plane towards the apical bridging Cl by 0.25 Å. The chelate bite angle in the five-membered ring formed by the N (pyridine) and N (imino ether group) is 79.43(8)°. The N–C, C–C, and C–N bond distances in the –N=C–C=N– fragment of the coordinated ligand are 1.254(3), 1.483(3), and 1.350(3) Å, respectively. The Cu–N (2) (pyridine) distance is considerably longer than the Cu–N(1) (imino ether group) distance. The former is 2.0642(18) Å whereas the latter is 1.972(2) Å. The difference may be due to rigidity of the bidentate ligand and the presence of bulky 2-butoxyethanol which enhanced π-backbonding in the Cu–N (1) (imine) bond [52–55]. The bridging Cu–Cl1 bonds are substantially different (2.7027(7) and 2.2748(6) Å) and are longer than the terminal Cu–Cl (2) bond (2.2375 (6) Å). These values are comparable to those observed in the binuclear copper chloride complexes [56, 57]. The Cl2–Cu1–Cl1i, Cl1–Cu1–Cl1i (bridge form), and Cl2–Cu1–Cl1 angles are 100.57(3)°, 96.89(2)°, and 94.98 (3)°, respectively. The metal–metal distance in the dichloro bridged complex is 3.317 Å, close to that found in other copper complexes containing similar bridging fragments (3.300 Å in dimeric complex formed by $CuCl_2$ with triphenyl-N-(6-methylpyridyl-2)phosphinimine [58], 3.5103 Å, $[Cu(ppmma)\text{-}Cl_2]_2$ [57], 3.358 Å in $[Ph_4P]_2[Cu_2Cl_6]$ [59] and 3.382 Å in $[Ph_4As]_2[Cu_2Cl_6]$ [60]).

As shown in figure 3, the intermolecular π–π contacts between the adjacent molecules related by the center of symmetry contribute to packing stabilization, where the distance between the two adjacent pyridine rings is 3.663 Å.

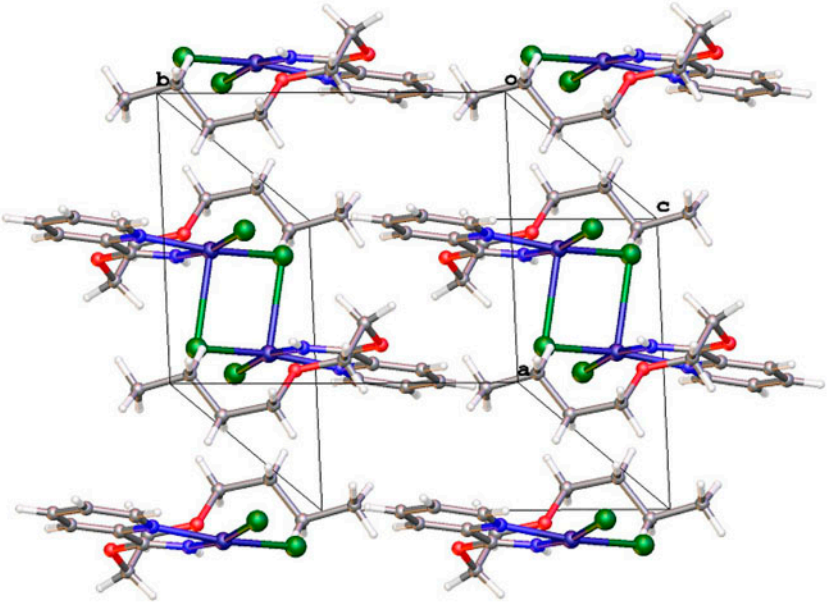

Figure 3. Packing diagram of **3** viewed along the *c*-axis.

3.5. *Powdered XRD studies*

XRD of **1** and **2** are depicted in Supplementary material. The observed diffraction data are given in Supplementary material. Using the program P-index, the computed cell parameters for **1** are $a = 11.7066$ Å, $b = 10.1841$ Å, $c = 8.6273$ Å, $\alpha = 76.167°$, $\beta = 95.905°$, $\gamma = 101.003°$ and cell volume = 978.6 Å^3. For **2**, $a = 10.9359$ Å, $b = 10.4847$ Å, $c = 9.7454$ Å, $\alpha = 81.454°$, $\beta = 96.915°$, $\gamma = 103.202°$ and cell volume = 1071.45 Å^3. These data of the complexes maintain triclinic systems. The crystallite size of the synthesized complex, D is determined by using Debye–Scherrer formula [61–63] given by

$$D = \frac{0.94\lambda}{\beta \cos\theta}$$

where β is the full width at half maximum of the predominant peak, θ is the diffraction angle and λ is the wavelength of light. The size of the crystallites of **1** and **2** are 75 and 76 nm, respectively.

3.6. *Thermogravimetric analysis*

Thermal decomposition behaviors of the complexes are characterized by TGA and DTA data from 30 to 850 °C in N_2 at heating rate of 10 °C min^{-1}. TGA, DTA curves of **2** and **3** are shown in Supplementary material. All three TGA curves show some common features and exhibit multi stage decomposition. In all the three spectra of the complexes there is no weight loss between 100 and 120 °C, showing no lattice water, confirmed from the crystal structure of **3**. The thermal decompositions occur gradually from 180 to 600 °C with an

endothermic peak at 190 °C corresponding to release of two (O-2-alkoxyethylpyridine-2-carboximidate) ligands and chloride of the complexes. The observed residue at 750 °C is CuO [64].

3.7. *DNA interaction study*

3.7.1. Electronic absorption titration. Figure 4 shows the absorption spectra of **2** in the presence and absence of increasing concentrations of DNA. For all the complexes, similar absorption bands at 272 nm with humps at 264 and 280 nm are observed. When increasing amounts of DNA are added, the copper(II) complexes show significant hyperchromic effect centered at 272 nm and the hump at 264 nm becomes more prominent (almost in the same level with that of the 272 nm peak). There is no change in the hump at 280 nm. Thus, the absorption bands of **1–3** are affected in the presence of DNA, with increase in absorption intensity (hyperchromism) and moderate blue shift (ca. 2 nm) of the peaks at 264 and 272 nm. Changes in the UV spectra of the complexes after mixing them with DNA suggest interaction of the complexes with DNA, due to formation of the complex with double helical DNA [65]. Therefore, the observed spectral changes show that **1–3** have an interaction with CT-DNA by partial or non-intercalative mode [42]. The values of K_b for **1–3** are 1.524×10^3, 5.587×10^3 and 6.362×10^3 $(ML^{-1})^{-1}$, respectively. The K_b values are much smaller than those reported for classical intercalators (EB–DNA, ~10^6 $(ML^{-1})^{-1}$) [66] and previously reported copper(II) complexes such as $[Cu_2(pdmaeox)(bpy)(H_2O)](pic)\cdot H_2O$ (K_b, 3.39×10^4 $(ML^{-1})^{-1}$) [67], $[Cu_2(oxbpa)(phen)(H_2O)](pic)\cdot 2H_2O$ (K_b, 1.50×10^5 $(ML^{-1})^{-1}$)) [68], $[Cu_4(oxbe)_2(bpy)_2](ClO_4)_2\cdot 2H_2O$ (K_b, 1.47×10^5 $(ML^{-1})^{-1}$) [69], $[Cu_2(heap)(H_2O)_2](pic)_2\cdot 2H_2O$ (K_b, 2.67×10^4 $(ML^{-1})^{-1}$) [70]), $[Cu_2(oxpep)(phen)]ClO_4$ (K_b, 4.50×10^5 $(ML^{-1})^{-1}$ [71] and $[Cu_2L(OAc)(CH_3OH)]\cdot CH_3OH$ (K_b, 1.16×10^5 $(ML^{-1})^{-1}$) [72] but similar level with those of the complexes $[Cu_2(L^1)_2(H_2O)]_\infty$ (K_b, 4.91×10^3 $(ML^{-1})^{-1}$) and $\{[Cu_2(L^2)_2(H_2O)]\cdot H_2O\}_\infty$ (K_b, 8.75×10^3 $(ML^{-1})^{-1}$) [73].

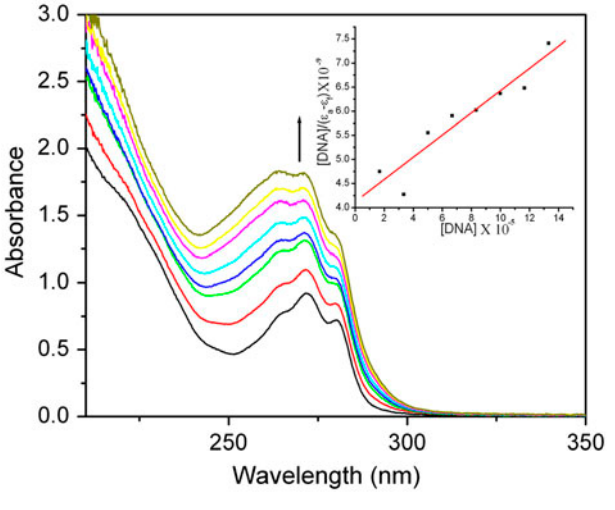

Figure 4. Absorption spectra in Tris buffer upon increasing concentrations of CT-DNA in the presence of the [Complex (**2**)] = 35 μM, [DNA] = 0–50 μM. Arrow shows the absorbance changes upon the increase in DNA concentration. Inset: plots of $[DNA]/(\varepsilon_a - \varepsilon_f)$ *vs.* [DNA] for CT-DNA with the complexes.

3.7.2. Thermal denaturation studies. The melting temperature of double-stranded DNA changes with different binding modes. The DNA melting temperature, T_m is the temperature where half of the total base pairs are unbound [74]. Generally, the melting temperature rises when metal complexes bind to DNA base pairs by intercalation causing stabilization of base stacking. A large change in the T_m of DNA is indicative of a strong interaction with DNA. The melting curves of CT-DNA in the absence and presence of varying concentrations of **1** are shown in figure 5. The melting temperature, T_m for DNA in the absence of the complex under our experimental condition is 74 °C. The observed melting temperatures for complexes are 75.3, 75.5, and 76 °C for **1**, **2,** and **3**, respectively. Thus, the minor changes in the melting temperature (ΔT_m) values of **1–3** suggest that DNA binding is primarily electrostatic or groove binding.

3.7.3. The EB fluorescence displacement experiments. Due to quenching of the solvent molecules, the fluorescence intensity of EB in tris buffer is not high and that of the DNA is also very low. However, the fluorescence intensity of EB is enhanced because of its intercalation into DNA base pairs. Thus, EB can be used to probe the interaction of complexes with DNA. The fluorescence intensity of EB–DNA adduct emission can be quenched by the addition of another DNA binding molecule due to the displacement of EB from DNA or photoelectron transfer mechanism [75]. In our experiment, as shown in figure 6, the fluorescence intensity of the EB bound to DNA at 597 nm showed significant decrease with increasing concentrations of **1–3**. The present observations indicate that the complexes may interact with DNA [76].

The fluorescence quenching of EB bound to DNA by the complexes is in agreement with the classical linear Stern–Volmer equation [77], $I_0/I = 1 + Kr$, where I_0 and I are the emission intensity in the absence and presence of the complex, respectively. K is the linear Stern–Volmer quenching constant and r is the ratio of the total concentration of the complex to that of DNA. The association constants (K_{app}) of **1–3** are 6.842×10^5, 7.26×10^5 and

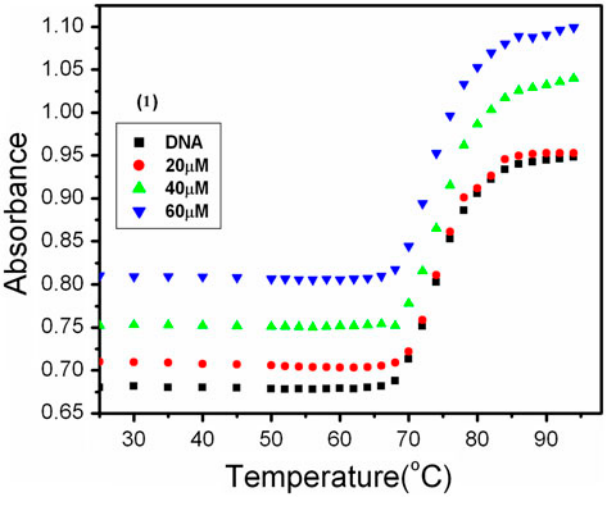

Figure 5. Thermal denaturation curves of CT-DNA in the absence and presence of varying amounts (20, 40, 60 μM) of **1**.

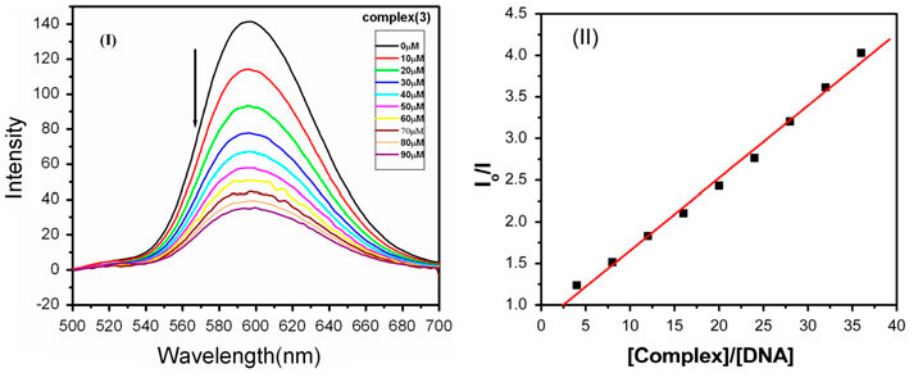

Figure 6. (I) Emission spectra EB bound to DNA in the presence of **3**. [EB] = 1.3 μM, [DNA] = 2.5 μM, [Complex] = 0–90 μM. The arrow shows the intensity changes on increasing the complex concentration. (II) Stern–Volmer plot of the complex.

8.125×10^5 $(ML^{-1})^{-1}$, respectively. The data suggest that the interaction with CT-DNA is stronger for **3** compared to **2** and **1**, which is also consistent with the absorption spectral and thermal denaturation studies; the binding capabilities are in the order **3** > **2** > **1**.

3.7.4. Electrochemical studies. A CV technique is employed to further explore the interaction of metal complexes with DNA assessed from the above spectral studies. Typical cyclic voltammograms of **2** at a scan rate of 20 mV are shown in Supplementary material. All the complexes show similar voltammograms, indicating two reduction peaks in the forward scan and two oxidation peaks in the reverse scan. The reduction peak (I) and the oxidation peak (I) are assigned to the Cu(II)/Cu(I) couple and the reduction peak (II) and oxidation peak (II) are assigned to the Cu(0)/Cu(I) couple. Variation of the peak potentials, as well as the peak currents in the absence and presence of CT-DNA indicate interaction between copper(II) complexes and the CT-DNA [78]. To understand the redox process and the binding mode of the complexes and CT-DNA, the separation between anodic and cathodic peak potentials, $\Delta E_p = E_{pa}E_{pc}$, ratio of the anodic and cathodic peak currents, I_{pc}/I_{pa}, and formal potential ΔE° (or voltammetric $E_{1/2} = [E_{pc} + E_{pa}]/2$) are calculated and summarized in table 5. For all three complexes, the peak-to-peak separation, ΔE_p is greater than 300 mV and current ratios I_{pc}/I_{pa} are away from unity. This suggests that the complexes show irreversible processes [42]. It is also observed that with the addition of (100 μM) CT-DNA the formal potential (or voltammetric $E_{1/2}$) shifted to more negative by (i) 28 mV [Cu(II)/Cu(I)], 11 mV [Cu(I)/Cu(0)] for **1**, (ii) 10 mV [Cu(II)/Cu(I)], 16 mV [Cu(I)/Cu(0)] for **2,** and (iii) 14 mV [Cu(II)/Cu(I)], 20 mV [Cu(I)/Cu(0)] for **3**. Thus, the complexes interact with the anionic phosphate of the DNA backbone via an electrostatic mode [79, 80].

3.7.5. Antimicrobial activity. The complexes are evaluated for *in vitro* antibacterial activity by using agar well diffusion. Complexes **2** and **3** show good antimicrobial activity against all the tested bacteria, whereas **1** does not exhibit antimicrobial activity. High inhibition is found against *S. paratyphi* (16 ± 0.22 mm) at 5 mg mL^{-1} (table 6). Antimicrobial activities are also reported as MIC values after overnight incubation. MIC of <0.07812 mg mL^{-1} is

Table 6. Antibacterial activities (zone of inhibition and MIC).

Complex	Bacteria	Inhibition zone, (mm) (mg mL^{-1})				Ciprofloxacin (100 μg mL^{-1})	MIC (mg mL^{-1})
		5	2.5	1.25	0.625		
1	*Proteus mirabilis*	–	–	–	–	16	>5
	Klebsiella pneumoniae	–	–	–	–	17	>5
	Escherichia coli	–	–	–	–	19	>5
	Salmonella paratyphi	–	–	–	–	19	>5
	Pseudomonas aeruginosa	12 ± 0.03	8 ± 0.2	–	–	20	0.625
2	*Proteus mirabilis*	14 ± 0.01	12 ± 0.14	8 ± 0.03	–	16	<0.15625
	Klebsiella pneumoniae	14 ± 0.32	11 ± 0.05	8 ± 0.2	–	17	0.15625
	Escherichia coli	–	–	–	–	19	>5
	Salmonella paratyphi	16 ± 0.22	14 ± 0.11	11 ± 0.2	9 ± 0.04	19	<0.07812
	Pseudomonas aeruginosa	–	–	–	–	20	>5
3	*Proteus mirabilis*	14 ± 0.4	12 ± 0.08	9 ± 0.03	–	16	0.15625
	Klebsiella pneumoniae	12 ± 0.12	10 ± 0.42	8 ± 0.2	–	17	>0.15625
	Escherichia coli	12 ± 0.22	9 ± 0.04	–	–	19	0.3125
	Salmonella paratyphi	12 ± 0.2	9 ± 0.03	8 ± 0.07	–	19	<0.3125
	Pseudomonas aeruginosa	–	–	–	–	20	>5

observed in *S. paratyphi* (table 6). The variation in the effectiveness of different complexes against different organisms depend either on differences in the permeability of the cells of the microbes or on difference in ribosome's of the microbes [81–83].

4. Conclusion

Three new chloride-bridged copper(II) complexes were synthesized and characterized. X-ray single crystal analysis of **3** reveals that the complex has a distorted square-pyramidal geometry. Based on similarity of IR spectra, electronic spectra, EPR, TGA–DTA, and powdered XRD pattern of **1** and **2** with that of **3** suggest that the complexes have the same structure. In addition, clear evidence of magnetic field induced molecular alignment in field-cooled samples of **2** and **3** are observed and the degrees of alignment are estimated to be 20%. DNA binding investigations by UV–visible, fluorescence, DNA melting temperature, and cyclic voltammetric studies show that the complexes interact with CT-DNA through non-intercalative binding mode and the binding capabilities are in the order **3** > **2** > **1**. Complexes **2** and **3** exhibit good antibacterial activities while **1** is inactive.

Supplementary material

Further information regarding the crystal structure determination and the crystallographic data (CIF file) of **3** has been deposited at the Cambridge Crystallographic Data Center (CCDC No. 928659). This data can be obtained free of charge via http://www.ccdc.cam.ac.uk/conts/retrieving.html, or from the Cambridge Crystallographic Data Center, 12 Union Road, Cambridge CB2 1EZ, UK; Fax: (+44) 1223336033; or E-mail: deposit@ccdc.cam.ac.uk

Acknowledgement

One of the authors (R.K. Bindiya Devi) gratefully acknowledges the financial support from the UGC-BSR fellowship.

References

[1] S.S. Wu, W.B. Yuan, H.Y. Wang, Q. Zhang, M. Liu, K.B. Yu. *J. Inorg. Biochem.*, **102**, 2026 (2008).
[2] A. Ray, G.M. Rosair, R. Kadam, S. Mitra. *Polyhedron*, **28**, 796 (2009).
[3] C. Metcalfe, J.A. Thomas. *Chem. Soc. Rev.*, **32**, 215 (2003).
[4] S. Dey, S. Sarkar, H. Paul, E. Zangrando, P. Chattopadhyay. *Polyhedron*, **29**, 1583 (2010).
[5] B.-F. Ye, Z.-J. Zhang, H.-X. Ju. *Chin. J. Chem.*, **23**, 58 (2005).
[6] H.M. Pinedo, J.H. Schornagel (Eds), *Platinum and other Metal Coordination Compounds in Cancer Chemotherapy*, Plenum Press, New York, Vol. 2 (1996).
[7] C.D. Lewis, U.K. Laemmli. *Cell*, **29**, 171 (1982).
[8] S. Hu, P. Furst, D. Hamer. *New Biol.*, **2**, 544 (1990).
[9] J.E. Weder, C.T. Dillon, T.W. Hambley, B.J. Kennedy, P.A. Lay, J.R. Biffin, H.L. Regtop, N.M. Davies. *Coord. Chem. Rev.*, **232**, 95 (2002).
[10] D.T. Minkel, L.A. Saryan, D.H. Petering. *Cancer Res.*, **38**, 124 (1978).
[11] D.T. Minkel, C. Chan-Stier, D.H. Petering. *Mol. Pharmacol.*, **12**, 1036 (1976).
[12] C.H. Chan-Stier, D. Minkel, D.H. Petering. *Bioinorg. Chem.*, **6**, 203 (1976).
[13] M. Mounir, J. Lorenzo, M. Ferrer, M.J. Prieto, O. Rossell, F.X. Avilès, V. Moreno. *J. Inorg. Biochem.*, **101**, 660 (2007).
[14] M. Ruíz, L. Perelló, J. Server-Carrió, R. Ortiz, S. García-Granda, M.R. Díaz, E. Cantón. *J. Inorg. Biochem.*, **69**, 231 (1998).
[15] A.M. Ramadan. *J. Inorg. Biochem.*, **65**, 183 (1997).
[16] X.L. Wang, H. Chao, H. Li, X.L. Hong, L.N. Ji, X.Y. Li. *J. Inorg. Biochem.*, **98**, 423 (2004).
[17] B. Selvakumar, V. Rajendiran, P.U. Maheswari, H.S. Evans, M. Palaniandavar. *J. Inorg. Biochem.*, **100**, 316 (2006).
[18] S. Dhar, M. Nethaji, A.R. Chakravarty. *J. Inorg. Biochem.*, **99**, 805 (2005).
[19] A. Bencini, E. Berni, A. Bianchi, C. Giorgi, B. Valtancoli, D.K. Chand, H.J. Schneider. *Dalton Trans.*, 793 (2003).
[20] D.K. Chand, H.J. Schneider, A. Bencini, A. Bianchi, C. Giorgi, S. Ciattini, B. Valtancoli. *Chemistry*, **6**, 4001 (2000).
[21] S. Dhar, D. Senapati, P.K. Das, P. Chattopadhyay, M. Nethaji, A.R. Chakravarty. *J. Am. Chem. Soc.*, **125**, 12118 (2003).
[22] P.R. Chetana, R. Rao, S. Saha, R.S. Policegoudra, P. Vijayan, M.S. Aradhya. *Polyhedron*, **48**, 43 (2012).
[23] G.W. Evans. *Nutr. Rev.*, **38**, 137 (1980).
[24] P.F.B. Barnard. *J. Chem. Soc. A*, 2140 (1969).
[25] S. Suzuki, M. Nakahara, K. Watanabe. *Bull. Chem. Soc. Jpn.*, **47**, 645 (1974).
[26] P. Segl'a, M. Jamnický. *Inorg. Chim. Acta*, **146**, 93 (1988).
[27] M. Jamnický, P. Segl'a, M. Koman. *Polyhedron*, **14**, 1837 (1995).
[28] Oxford Diffraction. *CrysAlis PRO and CrysAlis RED*, Oxford Diffraction Ltd., Abingdon (2010).
[29] G.M. Sheldrick. *Acta Cryst.*, **64**, 112 (2008).
[30] O.V. Dolomanov, L.J. Bourhis, R.J. Gildea, J.A.K. Howard, H. Puschmann. *J. Appl. Cryst.*, **42**, 339 (2009).
[31] J. Marmur. *J. Mol. Biol.*, **3**, 208 (1961).
[32] M.E. Reichmann, S.A. Rice, C.A. Thomas, P. Doty. *J. Am. Chem. Soc.*, **76**, 3047 (1954).
[33] M. Lee, A.L. Rhodes, M.D. Wyatt, S. Forrow, J.A. Hartley. *Biochemistry*, **32**, 4237 (1993).
[34] D. Greenwood. *Antimicrobial Chemotherapy. Part II: Laboratory Aspects of Antimicrobial Therapy*, Bailliere Tindall, London (1983).
[35] C.H. Collins, P.M. Lyne, J.M. Grange. *Microbiological Methods*, 6th Edn, Butterworths, London (1989).
[36] S. Kannan, M. Sivagamasundari, R. Ramesh, L. Yu. *J. Organomet. Chem.*, **693**, 2251 (2008).
[37] K.R. Cheruiyot, D. Olila, J. Kateregga. *Afr. Health Sci.*, **9**, S42–S46 (2009).
[38] B.J. Hathaway, D.E. Billing. *Coord. Chem. Rev.*, **5**, 143 (1970).
[39] A. Paulovicova, U. El-Ayaan, Y. Fukuda. *Inorg. Chim. Acta*, **321**, 56 (2001).
[40] M.J. Bew, R.J. Dudley, R.J. Fereday, B.J. Hathaway, R.C. Slade. *J. Chem. Soc. (A)*, 1437 (1971).
[41] M. Kohoutova, M. Kratsmar-Smogrovic, O. Svajlenova. *Chem. Zvesti.*, **29**, 373 (1975).
[42] S.D. Pramodini, R.K.D. Bindiya, N.D. Shantibala, L.S. Jaideva, R.K.S. Hemakumar. *Polyhedron*, **47**, 1 (2012).
[43] A.K. Patra, M. Nethaji, A.R. Chakravarty. *Dalton Trans.*, 2798 (2005).
[44] D. Kivelson, R. Neiman. *J. Chem. Phys.*, **35**, 149 (1961).

[45] J. Manonmani, R. Thirumurugan, M. Kandaswamy, M. Kuppayee, S.S.S. Raj, M.N. Ponnuswamy, G. Shanmugam, H.K. Fun. *Polyhedron*, **19**, 2011 (2000).
[46] J.R. Wasson, C. Trapp. *J. Phys. Chem.*, **73**, 3763 (1969).
[47] B.N. Figgis. *Introduction to Ligand Fields*, p. 295, Interscience, New York (1966).
[48] B.J. Hathaway. *Structure and Bonding*, Springer-Verlag, Heidelberg, Vol. 14, 60 (1973).
[49] G. Wilkinson. *Comprehensive Coordination Chemistry, The Synthesis Reactions, Properties and Applications of Coordination Compounds*, Vol. 5, p. 533, Pergamon Press, Cambridge (1987).
[50] M. Bose, K. Ohta, Y. Babu, M.D. Sastry. *Chem. Phys. Lett.*, **324**, 330 (2000).
[51] A.L. Sharma, I.O. Singh, M.A. Singh, H.R. Singh, R.M. Kadam, M.K. Bhide, M.D. Sastry. *Transition Met. Chem.*, **26**, 532 (2001).
[52] S. Seth, S. Chakraborty. *Acta Crystallogr., Sect. C*, **40**, 1530 (1984).
[53] G.V. Karunakar, N.R. Sangeetha, V. Susila, S. Pal. *J. Coord. Chem.*, **50**, 51 (2000).
[54] G.D. Storrier, S.B. Colbran, D.C. Craig. *J. Chem. Soc., Dalton Trans.*, 3011 (1997).
[55] A. Seal, S. Ray. *Acta Crystallogr., Sect. C*, **40**, 929 (1984).
[56] V.V. Davydov, V.I. Sokol, N.M. Kolyadina, E.I. Polyakova, S.V. Chernov, Yu.V. Shklyaev, V.S. Sergienko. *Russ. J. Inorg. Chem.*, **53**, 1573 (2008).
[57] H.W. Lee, N. Sengottuvelan, H.-J. Seo, J.S. Choi, S.K. Kang, Y.-I. Kim. *Bull. Korean Chem. Soc.*, **29**, 1711 (2008).
[58] R.U. Amanov, D.V. Tolkachev, M.Yu. Antipin, A.A. Khodak, Kh.T. Sharipov, Yu.T. Struchkov, M.I. Kabachnik. *Russ. Chem. Bull.*, **42**, 295 (1993).
[59] M. Textor, E. Dubler, H.R. Oswald. *Inorg. Chem.*, **13**, 1361 (1974).
[60] R.D. Willett, C. Chow. *Acta Crystallogr.*, **30B**, 207 (1974).
[61] B.E. Warren. *X-ray Diffraction*, p. 253, Dover, New York (1990).
[62] B. Prathima, Y.S. Rao, G.N. Ramesh, M. Jagadeesh, Y.P. Reddy, P.V. Chalapathi, A.V. Reddy. *Spectrochim. Acta Part A*, **79**, 39 (2011).
[63] R.K.D. Bindiya, S.D. Pramodini, R.K.S. Hemakumar. *Spectrosc. Lett.*, **45**, 93 (2012).
[64] B.M. Kukovec, Z. Popovic, G. Pavlovic. *Acta Chim. Slov.*, **55**, 779 (2008).
[65] N.M. El-Metwaly. *Transition Met. Chem.*, **32**, 88 (2007).
[66] J.B. LePecq, C. Paoletti. *J. Mol. Biol.*, **27**, 87 (1967).
[67] H.H. Lu, Y.T. Li, Z.Y. Wu, K. Zheng, C.W. Yan. *J. Coord. Chem.*, **64**, 1360 (2011).
[68] X.L. Wang, M. Jiang, Y.T. Li, Z.Y. Wu, C.W. Yan. *J. Coord. Chem.*, **66**, 1985 (2003).
[69] X.W. Li, M. Jiang, Y.T. Li, Z.Y. Wu, C.W. Yan. *J. Coord. Chem.*, **63**, 1582 (2010).
[70] X.W. Zhang, Y.J. Zheng, Y.T. Li, Z.Y. Wu, C.W. Yan. *J. Coord. Chem.*, **63**, 2985 (2010).
[71] S.H. Cui, M. Jiang, Y.T. Li, Z.Y. Wu, X.W. Li. *J. Coord. Chem.*, **64**, 4209 (2011).
[72] Y. Mei, J.J. Zhou, H. Zhou, Z.Q. Pan. *J. Coord. Chem.*, **65**, 643 (2012).
[73] C. Gao, X. Ma, J. Lu, Z. Wang, J. Tian, S. Yan. *J. Coord. Chem.*, **64**, 2157 (2011).
[74] Y.J. Liu, H. Chao, L.F. Tan, Y.X. Yuan, W. Wei, L.N. Ji. *J. Inorg. Biochem.*, **99**, 530 (2005).
[75] R. Indumathy, S. Radhika, M. Kanthimathi, T. Weyhermuller, B.U. Nair. *J. Inorg. Biochem.*, **101**, 434 (2007).
[76] J. Liu, T. Zhang, T. Lu, L. Qu, H. Zhou, Q. Zhang, L. Ji. *J. Inorg. Biochem.*, **91**, 269 (2002).
[77] J.R. Lakowicz, G. Weber. *Biochemistry*, **12**, 4161 (1973).
[78] Z.Q. Liu, Y.T. Li, Z.Y. Wu, S.F. Zhang. *Inorg. Chim. Acta*, **362**, 71 (2009).
[79] M.T. Carter, M. Rodriguez, A.J. Bard. *J. Am. Chem. Soc.*, **111**, 8901 (1989).
[80] K. Abdi, H. Hadadzadeh, M. Salimi, J. Simpson, A.D. Khalaji. *Polyhedron*, **44**, 101 (2012).
[81] N. Sarin, S. Arslan, E. Logolu, L. Sakiyan. *J. Sci.*, **16**, 283 (2003).
[82] C. Jayabalakrishnan, K. Natarajan. *Transition Met. Chem.*, **27**, 75 (2002).
[83] A.S. Gaballa, M.S. Asker, A.S. Barakat, S.M. Teleb. *Spectrochim. Acta Part A*, **67**, 114 (2007).